Journal of *Marine Science and Engineering*

MDPI

Article

A Novel Cooperative Localization Algorithm Based on LSTM and Factor Graph for AUV Swarms

Tong Sun, Weiming Xu *, Yisong Deng and Jinyang Luo

Department of Oceanography and Hydrography, Dalian Naval Academy, Dalian 116018, China; 18595453351@163.com (T.S.); 13247003755@163.com (Y.D.); 17336610291@163.com (J.L.)
* Correspondence: xwm921@163.com

Abstract

To address localization error accumulation in autonomous underwater vehicle (AUV) swarms due to underwater acoustic communication interruptions, this paper proposes a cooperative localization method that integrates Long Short-Term Memory (LSTM) prediction and factor graph optimization. During the real-time stage, each AUV uses a trained LSTM to predict observations, ensuring the Unscented Kalman filter (UKF) maintains continuous state estimation during interruptions and mitigates error accumulation. During the post-processing stage, a factor graph comprising motion model factors, cooperative observation factors, and LSTM prediction factors is constructed on the AUV swarm master node. By adaptively switching factor types based on communication status, global nonlinear optimization is performed on the AUV states. Simulation results show that compared with UKF + LSTM, the proposed method reduces the Average Localization Error (ALE) by 55% and the Root Mean Square Error (RMSE) by 60%; compared with the Rauch–Tung–Striebel (RTS) smoothing algorithm, it reduces the ALE by 36% and the RMSE by 44%. This fully verifies that the strategy combining real-time state maintenance and post-processing global optimization can more effectively correct AUV localization errors in communication-interrupted regions. Experiments under different communication interruption durations further confirm the robustness of the proposed algorithm, with the maximum error-to-range ratio remaining below 0.2% of the range.

Keywords: autonomous underwater vehicle swarm; cooperative localization; Long Short-Term Memory; factor graph

1. Introduction

Autonomous underwater vehicles (AUVs), with their high degree of autonomy, excellent environmental adaptability, and superior stealth capabilities [1], play an irreplaceable role in marine scientific research and resource development, such as seabed topography mapping and marine resource exploration, as well as in military operations, including target detection and underwater information warfare [2]. They have thus become a core component of the current marine technology system [3,4]. As underwater exploration missions grow increasingly complex, individual AUVs are constrained by factors such as payload capacity, operational efficiency, and system robustness, making it difficult for them to meet the demands of diverse and high-intensity missions. Consequently, AUV swarm cooperative localization technology based on acoustic communication networks has emerged. By employing acoustic communication to determine relative distances and

Check for updates

Academic Editor: Jiang Zhu

Received: 24 April 2026
Revised: 14 June 2026
Accepted: 17 June 2026
Published: 2 July 2026

Copyright: © 2026 by the authors. Licensee MDPI, Basel, Switzerland. This article is an open access article distributed under the terms and conditions of the Creative Commons Attribution (CC BY) license.

bearings between AUVs, and to facilitate information exchange and the sharing of navigation resources, the entire localization system gains enhanced fault tolerance, robustness, and stability, achieving a synergistic effect where "1 + 1 > 2" [5]. Within this cooperative framework, high-precision cooperative localization capability serves as the foundation and prerequisite for effective collaboration among the AUV swarm.

In complex marine environments, underwater acoustic channels are marked by severe multipath effects, limited bandwidth, and frequent communication interruptions [6], which prevent the AUV swarm from communicating effectively for extended periods. In such circumstances, relying solely on filtering algorithms for position estimation leads to rapid divergence of localization errors due to a lack of measurement updates, making it difficult to meet the requirements for long-duration, high-precision operations [7]. To address this issue, researchers have introduced artificial intelligence methods from various perspectives, including environmental adaptability, sensor fusion, and algorithmic efficiency. Xu [8] proposed a cooperative localization method based on an Adaptive Neuro-Fuzzy Inference System (ANFIS) and Cubic Kalman Filtering. This method predicts acoustic ranging errors online and corrects localization anomalies in real time. Li [9] designed a Convolutional Neural Network (CNN)-based LSTM model to address communication delays between master and slave AUVs within a swarm. Xu [10] proposed a master–slave AUV cooperative navigation model that improves the robust Cubature Kalman Filter algorithm by introducing maximum information potential to resolve the cooperative localization problem when the slave AUV's compass fails. Sun [11] proposed a cooperative localization algorithm for AUV swarms based on LSTM-assisted UKF. By incorporating LSTM's temporal prediction capabilities into the nonlinear filtering framework, the algorithm reduces reliance on continuous observations and designs localization strategies for different communication interruption scenarios. However, these intelligent models essentially belong to real-time estimation frameworks; although they can provide predictions during periods of no observation, errors still gradually accumulate as communication interruptions persist due to inherent model errors, discrepancies between the training data and the real environment, and the propagation of uncertainty during the prediction process.

To mitigate error accumulation in real-time estimation frameworks, current research typically employs post-processing correction, using historical data to refine localization results after the task has been completed. Zhang [12] proposed the STEKF-RTS algorithm, which eliminates the ratio term in the traditional velocity error equation by defining state transition rates during forward filtering and subsequently reconstructs underwater tracks for the AUV using RTS smoothing. Luo [13] proposed an InRTS smoothing algorithm with a state space defined as a matrix Lie group, fully employing the precision of state equations on matrix Lie groups and the advantage that the Jacobian matrix of the left-invariant Extended Kalman Filter (EKF) is independent of the state estimate. Dong [14] adopted a navigation information inversion approach, correcting the cumulative localization error of the master AUV by combining forward and inverse calculations. Wu [15] proposed a post-processing smoothing scheme that fuses RTS and FBC, significantly improving the underwater localization accuracy of AUVs. Ma [16] employed a factor graph post-processing method, achieving high-precision fusion and solution of multi-source asynchronous navigation information for AUVs through equivalent IMU dimensionality reduction and bidirectional message smoothing. These methods all address single-AUV systems independently; during the optimization process, they use only the kinematic and observation data of a single AUV, failing to fully leverage cooperative constraints such as relative ranging between members and communication topology during AUV swarm operations.

As a probabilistic graphical model, the factor graph provides an ideal framework for integrating multi-source information and is well suited for addressing swarm-based coop-

erative localization problems [17]. This framework enables unified modeling of the pose nodes of multiple AUVs on the master node and explicitly expresses the relative constraints among members through binary factors, thereby fully leveraging cooperative information in swarm operations [18]. To this end, this paper adopts the factor graph framework to uniformly model AUV motion models, observation information, and swarm cooperative constraints, with a particular focus on addressing the accumulation of localization errors during communication interruptions. Unlike existing methods that merely use LSTM prediction as a supplementary input for real-time estimation, this paper integrates the temporal prediction capability of LSTM into the factor graph framework, adaptively switching factor types according to communication conditions, when communication is normal, cooperative observation factors are introduced to constraints using relative observations between AUVs; during communication interruptions, incorporating the LSTM network's predicted values and their uncertainties as constraint factors into the factor graph, effectively suppressing divergence of localization errors. Compared with methods that only use RTS smoothing, which cannot exploit cooperative constraints or pure factor graph, which lacks effective observations during communication interruptions, the proposed LSTM + FG framework simultaneously addresses the two key issues of real-time prediction during interruptions and global cooperative optimization. The primary contributions of this paper are as follows:

1. A cooperative localization scheme integrating LSTM and factor graph is proposed, which combines online real-time localization with offline post-processing optimization. Filtering continuity is maintained during communication interruptions, and global correction of AUV swarm localization trajectories is achieved using complete historical data.
2. A multi-source information fusion factor graph is constructed to integrate motion model data, master–slave cooperative observations, and LSTM predictions. Global non-linear least-squares optimization is employed to fully exploit swarm cooperative in-formation, improving localization accuracy under communication interruptions.
3. Monte Carlo Dropout (MC Dropout) is introduced to quantify LSTM prediction uncertainty, and the resulting covariance matrix is used as adaptive weights for factor graph optimization. Unreliable predictions are effectively suppressed, enhancing both localization accuracy and robustness in post-processing.

2. System Modeling

2.1. Motion Model

In practical applications, the underwater motion of an AUV can be described using a three-dimensional motion model. Figure 1 shows a schematic diagram of the AUV in both the inertial coordinate system and the carrier coordinate system.

For the i AUV in the swarm, its state vector in the navigation coordinate system is defined as:

$$X_i = \left[x_i, y_i, z_i, v_{x,i}, v_{y,i}, v_{z,i}, a_{x,i}, a_{y,i}, a_{z,i}, \phi_i, \theta_i, \varphi_i\right]^{\mathrm{T}} \tag{1}$$

where X_i is the state vector of the i AUV. (x_i, y_i, z_i) represents the three-dimensional position coordinates in the navigation coordinate system; $(v_{x,i}, v_{y,i}, v_{z,i})$ represents the velocity components along the three axes; $(a_{x,i}, a_{y,i}, a_{z,i})$ represents the disturbance acceleration components used to compensate for dynamic modeling errors; and $(\phi_i, \theta_i, \varphi_i)$ represents the attitude angles, specifically roll, pitch, and yaw, all measured in degrees (°). These must be converted to radians when performing trigonometric calculations. At a sampling interval of Δt, the system state equation can be expressed as:

$$X_{i,k+1} = f(X_{i,k}, u_{i,k}) + w_{i,k} \tag{2}$$

where $f(\cdot)$ represents the nonlinear state transition function; the control input $u_{i,k} = [(f_k^b)^{\mathrm{T}}, (\omega_k^b)^{\mathrm{T}}]^{\mathrm{T}}$ consists of the specific force vector $f_k^b = [f_{x,k}^b, f_{y,k}^b, f_{z,k}^b]^{\mathrm{T}}$ and the angular velocity vector $\omega_k^b = [\omega_{x,k}^b, \omega_{y,k}^b, \omega_{z,k}^b]^{\mathrm{T}}$ measured by the IMU in the vehicle carrier coordinate system. The process noise vector $w_{i,k}$ is assumed to be white Gaussian noise with a covariance matrix $Q = diag(Q_p, Q_v, Q_a, Q_\Theta)$,where each sub-matrix represents the noise variance element corresponding to each state component. The specific form of the state transition function $f(\cdot)$ is:

$$\begin{cases} p_{k+1} = p_k + v_k \Delta t + \frac{1}{2}(R_b^n(\Theta_k) f_k^b + a_k)\Delta t^2 \\ v_{k+1} = v_k + (R_b^n(\Theta_k) f_k^b + a_k)\Delta t \\ a_{k+1} = a_k + w_{a,k} \\ \Theta_{k+1} = \Theta_k + E(\Theta_k)\omega_k^b \Delta t \end{cases} \tag{3}$$

where $p_k = [x_k, y_k, z_k]^{\mathrm{T}}$, $v_k = \left[v_{x,k}, v_{y,k}, v_{z,k}\right]^{\mathrm{T}}$, $a_k = \left[a_{x,k}, a_{y,k}, a_{z,k}\right]^{\mathrm{T}}$ and $\Theta_k = [\phi_k, \theta_k, \varphi_k]^{\mathrm{T}}$ represent the sub-vectors of position, velocity, disturbance acceleration, and attitude angles at time step k, respectively. $w_{a,k}$ denotes the random driving noise vector of the disturbance acceleration. $R_b^n(\Theta)$ is the rotation matrix from the carrier coordinate system to the navigation coordinate system, determined by the attitude angles at time k:

$$R_b^n(\Theta) = \begin{bmatrix} \cos\varphi\cos\theta & \cos\varphi\sin\theta\sin\phi - \sin\varphi\cos\phi & \cos\varphi\sin\theta\cos\phi + \sin\varphi\sin\phi \\ \sin\varphi\cos\theta & \sin\varphi\sin\theta\sin\phi + \cos\varphi\cos\phi & \sin\varphi\sin\theta\cos\phi - \cos\varphi\sin\phi \\ -\sin\theta & \cos\theta\sin\phi & \cos\theta\cos\phi \end{bmatrix} \tag{4}$$

$E(\Theta)$ denotes the Euler angular velocity transformation matrix, which maps the carrier angular velocity to the attitude angular velocity:

$$E(\Theta) = \begin{bmatrix} 1 & \sin\phi\tan\theta & \cos\phi\tan\theta \\ 0 & \cos\phi & -\sin\phi \\ 0 & \sin\phi/\cos\theta & \cos\phi/\cos\theta \end{bmatrix} \tag{5}$$

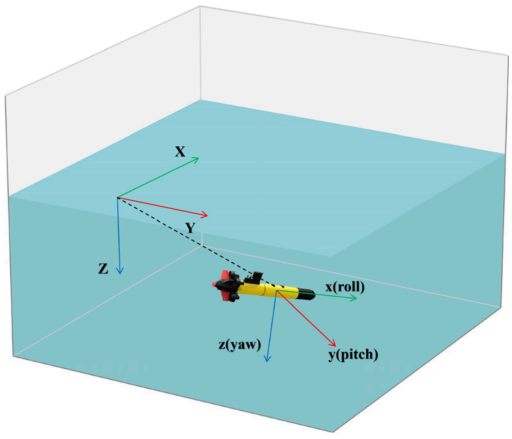


Figure 1. AUV Motion Coordinate System.

2.2. Measurement Model for AUV Swarm Cooperative Localization Systems

Considering localization device configuration, mission needs, system complexity, and cost, cooperative localization for AUV swarms mainly includes master–slave, parallel, surface-vehicle-assisted, and single-beacon-assisted methods. The master–slave architecture is the most mature and widely used for AUV swarms due to its simple structure, ease of implementation, cost control, and suitability for small- to medium-sized swarms. This

paper employs a master–slave cooperative localization method for AUVs. The master AUV is equipped with high-precision navigation and localization equipment and obtains its precise position through sensors such as GNSS smart buoys (GIBs), inertial navigation systems (INS), or Doppler velocity loggers (DVLs). The slave AUV is equipped with a lower-precision dead-reckoning system and estimates its position using relative measurements and cooperative localization algorithms [19]. The system model is shown in Figure 2.

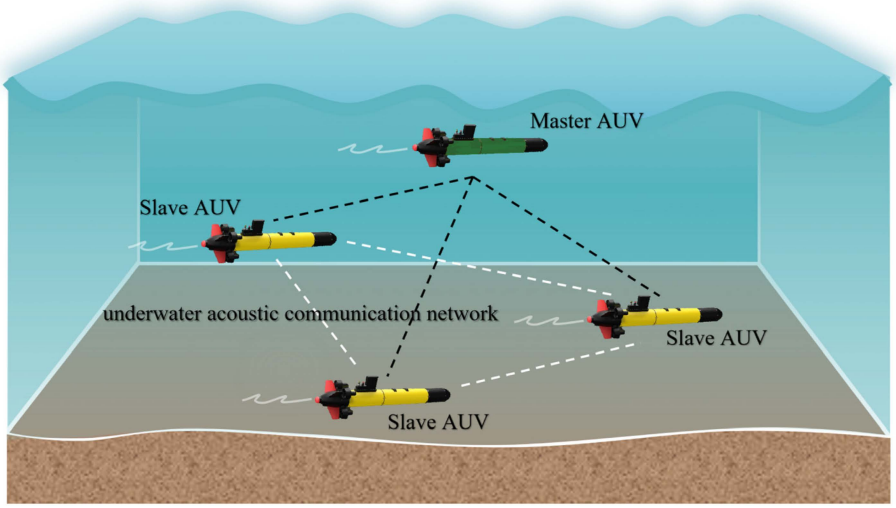


Figure 2. Schematic diagram of the AUV swarm cooperative localization system.

The relative distance r, azimuth α, and elevation angle β between the master AUV and the slave AUV, obtained through acoustic communication, can be expressed as:

$$Z_{ms,k} = \begin{bmatrix} r_{ms,k} \\ \alpha_{ms,k} \\ \beta_{ms,k} \end{bmatrix} = h(X_{m,k}, X_{s,k}) + \nu_{ms,k} \tag{6}$$

The concrete mathematical elements of the nonlinear observation function $h(\cdot)$ are expressed as follows:

$$\begin{cases} r_{ms,k} = \sqrt{(x_{s,k} - x_{m,k})^2 + (y_{s,k} - y_{m,k})^2 + (z_{s,k} - z_{m,k})^2} \\ \alpha_{ms,k} = \text{atan2}(y_{s,k} - y_{m,k}, x_{s,k} - x_{m,k}) \\ \beta_{ms,k} = \text{atan2}\left(z_{s,k} - z_{m,k}, \sqrt{(x_{s,k} - x_{m,k})^2 + (y_{s,k} - y_{m,k})^2}\right) \end{cases} \tag{7}$$

where $(x_{m,k}, y_{m,k}, z_{m,k})$ and $(x_{s,k}, y_{s,k}, z_{s,k})$ denote the three-dimensional position elements of the master AUV and the slave AUV at time step k in the navigation coordinate system, respectively. $\nu_{ms,k}$ represents the measurement noise at time k, which is assumed to follow a Gaussian distribution with probability distribution given by $\nu_{ms,k} \sim N(0, R_{ms,k})$.

3. UKF + LSTM Real-Time Cooperative Localization

3.1. Unscented Kalman Filter Design

Under normal communication conditions, methods such as the EKF and the UKF handle noise, nonlinearities, and sensor uncertainties, enabling position estimation for AUVs [20]. The UKF achieves higher state estimation accuracy than the EKF [21,22], thereby providing more reliable localization. Thus, this paper adopts the UKF as the base filter for real-time cooperative localization. The unscented transformation approximates the

posterior probability density function for nonlinear systems. It can also approximate the mean and variance of the state for Gaussian linear systems with second-order or higher accuracy. This approach is suitable for real-time filtered localization in cooperative localization systems for AUV swarms relying on underwater acoustic communication during normal operation [23]. Figure 3 shows the specific implementation process.

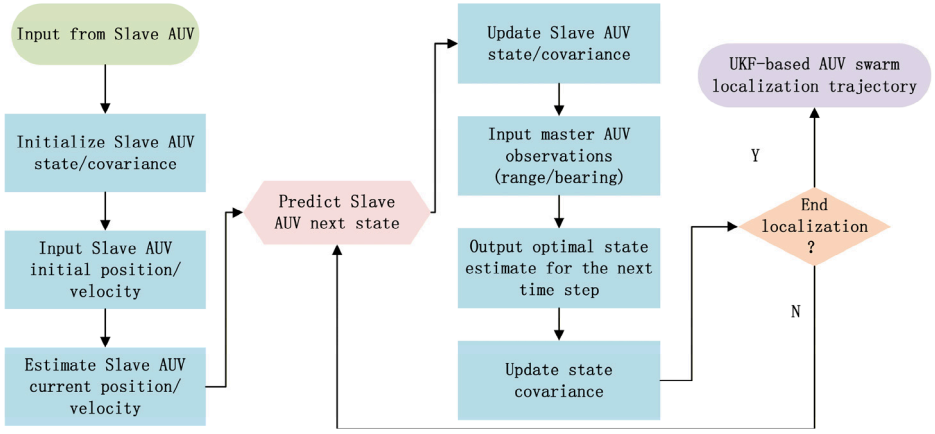


Figure 3. Flowchart of the UKF Algorithm Implementation.

When communication is interrupted, the system cannot obtain real-time observations, leading to rapid error accumulation until divergence occurs. Therefore, this paper introduces an LSTM network to learn AUV dynamic behavior using historical measurement sequences accumulated during periods of normal communication, thereby providing virtual observations to the swarm during communication interruptions.

3.2. Monte Carlo Dropout-Based LSTM Network

LSTM effectively captures long-term dependencies in time series through its gating mechanism, mitigating the vanishing gradient problem to some extent. It is suitable for processing and forecasting time-series data characterized by long intervals and delays [24]. Its structure is shown in Figure 4.

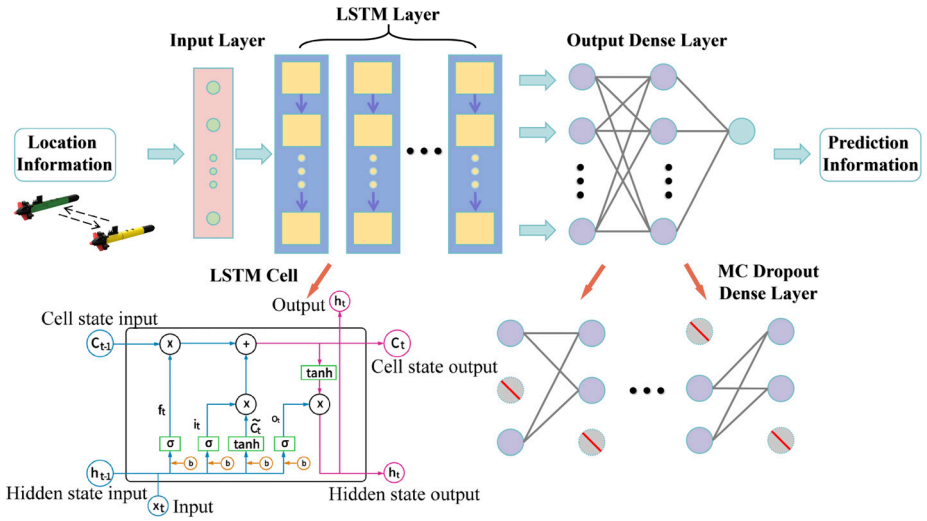


Figure 4. LSTM Network Architecture.

The input to the network is a sequence of measurements $\{Z_{t-k+1}, \cdots, Z_t\}$ from the past k time steps, and the output is a predicted measurement $\hat{Z}_{t+1}$ for the next time step. The forward propagation in an LSTM can be expressed as:

$$h_t, c_t = LSTM(x_t, h_{t-1}, c_{t-1}; W_{lstm}) \tag{8}$$

where x_t is the input vector at the current time step, while h_t and c_t denote the hidden state and cell state vectors, respectively. W_{lstm} represents the internal gating weight matrices of the LSTM cell. Since the hidden state h_t is a highly abstract, non-physical feature vector, an output dense layer must be appended to map these hidden features back into the physical measurement space, thereby synthesizing the final virtual observation vector:

$$\hat{Z}_{t+1} = W_0 h_t + b_0 \tag{9}$$

where $\hat{Z}_{t+1} = [\hat{r}, \hat{\alpha}, \hat{\beta}]^{\mathrm{T}} \in \mathrm{R}^{3\times 1}$ is the predicted virtual measurement vector element for the next time step, containing the predicted relative range, azimuth, and elevation angle, respectively. $h_t \in \mathrm{R}^{m\times 1}$ represents the hidden state vector element output by the LSTM cell (m denotes the number of hidden units). $W_0 \in \mathrm{R}^{3\times m}$ defines the output weight matrix element, and $b_0 = \mathrm{R}^{3\times 1}$ represents the output bias vector element.

All the network parameters, $W = \{W_{lstm}, W_0, b_0\}$, are trained using the mean squared error (MSE) loss function. The training data are derived from historical measurements accumulated during periods of normal communication and are continuously updated using an online sliding window approach. To quantify the LSTM model's prediction reliability, the Monte Carlo Dropout (MC Dropout) method [25] is introduced to regularize the LSTM network. When generating virtual measurements, N random forward passes are performed on the same input to obtain a set of predicted values $\left\{\hat{z}_{t+1}^{(1)}, \cdots, \hat{z}_{t+1}^{(N)}\right\}$, and the mean of the virtual measurement values is:

$$\bar{z}_{t+1} = \frac{1}{N}\sum_{i=1}^{N} \bar{z}_{t+1}^{(i)} \tag{10}$$

This uncertainty is represented by the covariance matrix:

$$P_{LSTM} = \frac{1}{N-1}\sum_{i=1}^{N} (\hat{z}_{t+1}^{(i)} - \bar{z}_{t+1})(\hat{z}_{t+1}^{(i)} - \bar{z}_{t+1})^{\mathrm{T}} \tag{11}$$

This covariance matrix dynamically reflects the LSTM's confidence in predicting the output at the current time step, providing an adaptive weighting basis for subsequent factor graph optimization.

3.3. UKF + LSTM Fusion Localization Under Communication Interruption

During normal communication, the system performs localization via the UKF and updates its state using actual observation data. At the same time, the observation data is stored in a historical sequence buffer for training the LSTM network. When communication is interrupted, the trained LSTM network generates virtual observations from historical observation sequences and feeds them to the UKF to replace missing actual observations. This design effectively suppresses the propagation of localization errors while maintaining filtering continuity. The algorithm framework is shown in Figure 5.

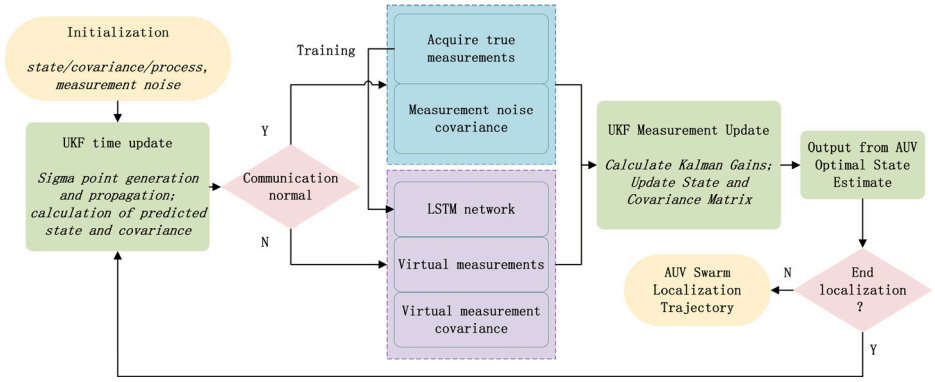


Figure 5. Framework diagram of the UKF + LSTM real-time localization algorithm.

4. Cooperative Localization Correction Based on Factor Graph Optimization

4.1. Theory of Factor Graph Optimization

A factor graph is a bipartite graph used to represent the factorization of multivariate functions, consisting of variable nodes and factor nodes [26]. Suppose the global function can be decomposed into the product of several local functions:

$$f(X) = \prod_i f_i(X_i) \tag{12}$$

where $X = \{x_1, x_2, \cdots, x_n\}$ denotes the set of variables, and each local function $f_i(X_i)$ depends on a subset of variables $X_i \subseteq X$. In a factor graph, a variable node represents an unknown variable, while a factor node represents a local function that imposes a constraint based on a subset of variables. Edges connect function nodes to the variable nodes they depend on.

Building upon this framework, in the AUV swarm cooperative localization problem, variable nodes correspond to the position states of AUVs at each time step, while factor nodes represent constraints such as motion models, relative observations, and prior information. Using a factor graph, the state estimation problem can be transformed into a maximum a posteriori estimation problem:

$$\hat{X} = \underset{X}{\operatorname{argmax}}\, p(X|Z) \propto \prod_k f_k(X_k) \tag{13}$$

Taking the negative logarithm is equivalent to solving a nonlinear least-squares problem. Unlike traditional filtering algorithms, factor graphs can perform batch-state smoothing across the entire time window [27]. To address the challenge of obtaining cooperative observations during communication interruptions in an AUV swarm, this paper constructs a factor graph model incorporating multi-source information to achieve global optimization of the slave AUV position sequences.

4.2. Factor Graph Construction

Let the communication interruption interval be $\mathrm{T} = \{0, 1, \cdots, k\}$, containing $K + 1$ discrete time points. For each time point k, define the position variable of the slave AUV as:

$$X_k = [p_k^{\mathrm{T}}, v_k^{\mathrm{T}}, a_k^{\mathrm{T}}]^{\mathrm{T}} \tag{14}$$

where p_k, v_k and a_k represent the AUV's three-dimensional position, velocity, and acceleration, respectively. The UKF + LSTM algorithm employs a comprehensive model that

incorporates pose information, while the factor graph corrects position errors through dimensionality reduction. All variables form the set $\chi = \{X_0, X_1, \cdots, X_k\}$.

1. Priori factor

To ensure that factor graph optimization has a unique solution and to establish a fixed initial state that serves as a reference anchor for the entire motion, a prior factor is introduced:

$$f_{prior}(X_0) \propto \exp(-\frac{1}{2} \parallel X_0 - \hat{X}_0 \parallel^2_{P_0}) \tag{15}$$

The prior information for the initial state is provided by external sensors such as GNSS and depth sensors, and follows a Gaussian distribution $N(\hat{X}_0, P_0)$. Here, $\hat{X}_0$ represents the initial state estimate, and P_0 represents the covariance matrix.

2. Motion factor

There are kinematic constraints between adjacent time steps in the AUV motion. At time k the velocity is v_k and the acceleration is a_k, the motion model is:

$$\begin{aligned} p_{k+1} &= p_k + v_k \Delta t + \tfrac{1}{2} a_k \Delta t^2 + \varepsilon_p \\ v_{k+1} &= v_k + a_k \Delta t + \varepsilon_v \\ a_{k+1} &= a_k + \varepsilon_a \end{aligned} \tag{16}$$

where Δt is the sampling interval, and ε_p, ε_v, ε_a represent process noise, which is assumed to follow a zero-mean Gaussian distribution with covariance matrices $\sigma_p^2 \mathrm{I}_3$, $\sigma_v^2 \mathrm{I}_3$ and $\sigma_a^2 \mathrm{I}_3$, respectively. The motion model here is not a true equation of motion. It is merely a constraint used to keep the trajectory smooth. the motion component residual is given by:

$$e_k^{motion} = \begin{bmatrix} p_{k+1} - p_k - v_k \Delta t - \frac{1}{2} a_k \Delta t^2 \\ v_{k+1} - v_k - a_k \Delta t \\ a_{k+1} - a_k \end{bmatrix} \tag{17}$$

The residuals follow a Gaussian distribution with a mean of zero, and their covariance matrix is a constant block diagonal matrix:

$$Q_{motion} = \begin{bmatrix} \sigma_p^2 I_3 & 0 & 0 \\ 0 & \sigma_v^2 I_3 & 0 \\ 0 & 0 & \sigma_a^2 I_3 \end{bmatrix} \tag{18}$$

where I_3 represents a 3×3 identity matrix element, and σ_p^2,σ_v^2,σ_a^2 are the noise variance elements of the kinematic model. To link the state variables of the AUV at adjacent time steps and reflect the inertial constraints of the AUV's motion, the motion factor can be defined as:

$$f_{motion}(X_k, X_{k+1}) \propto \exp(-\frac{1}{2} \parallel e_k^{motion} \parallel^2_{Q_{motion}}) \tag{19}$$

3. Cooperative Observation Factor

In cooperative localization for an AUV swarm, each slave AUV obtains its distance, azimuth, and elevation relative to the master AUV via acoustic communication. When communication is normal and the corresponding ranging information is received at a given moment, the associated measurement function can be expressed as follows:

$$h(p_k) = \begin{bmatrix} \parallel p_k - m_k \parallel_2 \\ \mathrm{atan2}(y_k - m_{y,k}, x_k - m_{x,k}) \\ \mathrm{atan2}\left(z_k - m_{z,k}, \sqrt{(x_k - m_{x,k})^2 + (y_k - m_{y,k})^2}\right) \end{bmatrix} \tag{20}$$

where m_k represents the master AUV position, provided by high-precision navigation equipment. The measurement noise is a zero-mean Gaussian white noise sequence satisfying $v_k \sim N(0, R_{coop})$, calibrated based on sensor characteristics to reflect measurement uncertainty. The covariance matrix is expressed in diagonal form:

$$R_{coop} = diag(\sigma_r^2, \sigma_\alpha^2, \sigma_\beta^2) \tag{21}$$

The residual vector is:

$$e_k^{coop} = \begin{bmatrix} \| p_k - m_k \| - r_k^{meas} \\ \text{atan2}(y_k - m_{y,k}, x_k - m_{x,k}) - \alpha_k^{meas} \\ \text{atan2}\left(z_k - m_{z,k}, \sqrt{(x_k - m_{x,k})^2 + (y_k - m_{y,k})^2}\right) - \beta_k^{meas} \end{bmatrix} \tag{22}$$

Normalize the angular residuals:

$$normalize(\delta) = \text{atan2}(\sin\delta, \cos\delta) \tag{23}$$

Define the cooperative observation factor as:

$$f_{coop}(p_k) \propto \exp\left\{-\frac{1}{2} \| e_k^{coop} \|_{R_{coop}}^2\right\} \tag{24}$$

The cooperative observation factors described above primarily represent relative observational constraints between the master AUV and slave AUVs. If two slave AUVs within a swarm can also obtain relative distance, azimuth, and elevation through underwater acoustic communication, a similar definition of cooperative observation factors can be established for their relationship. Therefore, cooperative observation factors can be extended to describe relative observations between any two AUVs within a swarm capable of underwater acoustic communication. However, this paper focuses on integrating LSTM prediction with factor graph post-processing, with particular emphasis on addressing the accumulation of localization errors in individual slave AUVs during communication interruptions; therefore, it considers only the cooperative observation constraints between the master AUV and the slave AUVs.

4. LSTM Prediction Factor

During communication interruptions, the slave AUV completely loses external calibration information because no actual ranging data from the master AUV can be received. To suppress the rapid divergence of dead-reckoning localization errors, virtual measurements are generated from historical measurement sequences via the trained LSTM network and incorporated into the factor graph framework as an adaptive soft constraint.

Specifically, the LSTM network outputs the predicted virtual measurement vector for the next time step, denoted as $\bar{z}_{k+1} = [r, \alpha, \beta]^T$, where the individual elements r, α and β represent the predicted relative distance, azimuth, and elevation angle, respectively. To bridge the gap between the measurement space and the variable nodes (position states) in the factor graph, a coordinate reconstruction function $g(\cdot)$ is introduced to map the spherical virtual measurements to the relative Cartesian position increments $\Delta\hat{p} = [\Delta x, \Delta y, \Delta z]^T$:

$$\Delta\hat{p} = g(\bar{z}_{k+1}) \tag{25}$$

The concrete analytical elements of the reconstruction function $g(\cdot)$ re derived from the geometric relationship as follows:

$$\begin{cases} \Delta x = r\cos\beta\cos\alpha \\ \Delta y = r\cos\beta\sin\alpha \\ \Delta z = r\sin\beta \end{cases} \tag{26}$$

Based on this geometric reconstruction, the predicted absolute position of the slave AUV can be computed as $\hat{p}_{s,k} = p_{m,k} + \Delta\hat{p}$, where $p_{m,k}$ represents the known high-precision position element of the master AUV at time step k.

To accurately propagate the network's prediction uncertainty into the position state space, the pseudo-observation covariance matrix P_p in the position domain is derived using the first-order Taylor expansion and the covariance propagation law:

$$P_p = J_g P_{LSTM} {J_g}^{\mathrm{T}} \tag{27}$$

where $P_{LSTM} \in \mathrm{R}^{3\times3}$ represents the virtual measurement uncertainty covariance matrix dynamically estimated by MC Dropout in the observation space. $J_g \in \mathrm{R}^{3\times3}$ denotes the Jacobian matrix of the coordinate reconstruction function $g(\cdot)$ with respect to the virtual measurement vector $\bar{z}_{k+1}$. To explicitly describe the underlying components for correct engineering application, the complete mathematical structure of J_g is expanded as:

$$J_g = \frac{\partial g}{\partial \bar{z}_{k+1}} = \begin{bmatrix} \frac{\partial \Delta x}{\partial r} & \frac{\partial \Delta x}{\partial \alpha} & \frac{\partial \Delta x}{\partial \beta} \\ \frac{\partial \Delta y}{\partial r} & \frac{\partial \Delta y}{\partial \alpha} & \frac{\partial \Delta y}{\partial \beta} \\ \frac{\partial \Delta z}{\partial r} & \frac{\partial \Delta z}{\partial \alpha} & \frac{\partial \Delta z}{\partial \beta} \end{bmatrix} \tag{28}$$

By executing analytical differentiation on each geometric component, the precise matrix elements inside J_g are determined as:

$$J_g = \begin{bmatrix} \cos\beta\cos\alpha & -r\cos\beta\sin\alpha & -r\sin\beta\cos\alpha \\ \cos\beta\sin\alpha & r\cos\beta\cos\alpha & -r\sin\beta\sin\alpha \\ \sin\beta & 0 & r\cos\beta \end{bmatrix} \tag{29}$$

Through this explicit formulation, the factor graph optimization can dynamically scale the positional covariance elements based on the current baseline range r and angular geometry (α, β), avoiding isotropic misjudgments of tracking errors during communication interruptions. Accordingly, the residual error vector e_k^{lstm} for the LSTM prediction factor is defined as the geometric discrepancy between the optimized slave AUV position variable $p_{s,k}$ and the predicted position element:

$$e_k^{lstm} = p_{s,k} - (p_{m,k} + \Delta\hat{p}) \tag{30}$$

Finally, the LSTM prediction factor $f_{LSTM}(p_k)$ is formally written as:

$$f_{LSTM}(p_k) \propto \exp\left\{-\frac{1}{2} \parallel e_k^{lstm} \parallel^2_{R_{lstm}}\right\} \tag{31}$$

where $R_{lstm} = P_p$ acts as the time-varying, adaptive covariance matrix element that regulates the optimization weights of the variable nodes when acoustic communication is interrupted.

This factor therefore provides a weak constraint in the absence of actual range measurements. When combined with the motion factor and the cooperative observation factor, it completes the factor graph and enables the integration of multi-source information.

By taking the negative natural logarithm of the posterior probability to be maximized, obtained by multiplying the above factors, the optimization problem can be transformed into a nonlinear least-squares form:

$$\chi^* = \underset{\chi}{\operatorname{argmin}}(\| X_0 - \hat{X}_0 \|^2_{P_0} + \sum_{k=0}^{T-2} \| e_k^{motion} \|^2_{Q_{motion}} + \sum_{k=0}^{T-1} \| e_k^{obs} \|^2_{R_{obs}(c_k)}) \tag{32}$$

Among these, the cooperative observation factor and the LSTM prediction factor adaptively switch based on the communication state c_k.

$$e_k^{obs} = \begin{cases} e_k^{coop}, & c_k = 1 \\ e_k^{lstm}, & c_k = 0 \end{cases} \tag{33}$$

$$R_{obs} = \begin{cases} R_{coop}, & c_k = 1 \\ R_{lstm}, & c_k = 0 \end{cases} \tag{34}$$

The factor graph abstracts the AUV swarm's navigation state at i time step into variable nodes x_i. Sensor information is represented as factors f_{prior}, f_{motion} and f_{coop}, while predictions from the LSTM network are represented as factor f_{LSTM}. Figure 6 provides a simplified schematic: pink denotes the master AUV's state, blue marks the slave AUVs' states, the black dashed box indicates intervals of normal communication, and the red dashed box indicates intervals with communication interruption.

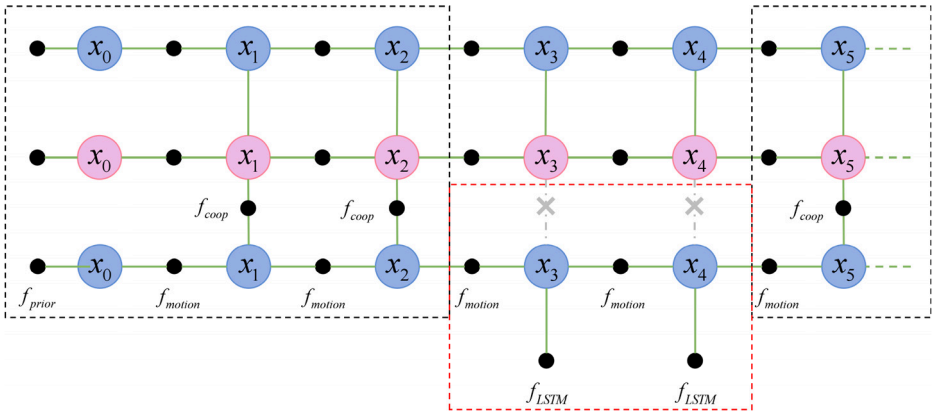


Figure 6. Schematic diagram of the simplified factor graph model.

The optimization problem is solved iteratively using the Levenberg–Marquardt algorithm [28]. By minimizing the weighted sum of squared errors, an optimal state sequence estimate for the slave AUV over the entire time window is obtained.

4.3. A Cooperative Localization Algorithm Based on LSTM and Factor Graph for AUVs

The cooperative localization method proposed in this paper has two stages: online filtering (Algorithm 1) and offline optimization (Algorithm 2).

Algorithm 1 constitutes the online stage and is based on a UKF fused with an LSTM. When communication is normal, it uses actual observations to update the filter and accumulate training data; when communication is interrupted, the LSTM network generates virtual observations to replace missing measurements, thereby maintaining filter continuity and outputting a real-time localization estimate sequence for the slave AUV.

Algorithm 1: UKF Real-Time Cooperative Localization Algorithm Based on LSTM Prediction (UKF + LSTM)

Input: State information of master AUV, initial state of slave AUV, historical measurement sequence
Output: Real-time localization estimation sequence of slave AUV $\{\hat{x}_0, \hat{x}_1, \cdots, \hat{x}_k\}$

While executing AUV swarm cooperative localization task **do**
  If $c_k = 1$ (communication is normal) **then**
    Use UKF to perform filtering estimation for slave AUV
    Generate Sigma points
    Time update: $\hat{x}_{k|k-1}$, $P_{k|k-1}$
    Measurement update:$\hat{x}_{k|k}$, $P_{k|k}$
    Store the current measurement into the historical buffer for online LSTM training
  Else if $c_k = 0$ (communication is interrupted) **then**
    Use the trained LSTM network to generate virtual measurement
      $\hat{Z}_{k+1} = W_0 h_k + b_0$, where $h_k, c_k = LSTM(x_k, h_{k-1}, c_{k-1}; W)$
      Calculate $\overline{Z}_{k+1}$ and P_{LSTM} using MC Dropout
    Take $\overline{Z}_{k+1}$ as the measurement input of UKF for update
  If communication is restored **do**
    Return to Step 2 to continue UKF filtering
End Return the real-time localization estimation sequence of slave AUV $\{\hat{x}_0, \hat{x}_1, \cdots, \hat{x}_k\}$

Algorithm 2 constitutes the offline post-processing stage. After obtaining the initial localization sequence, an adaptive factor graph model is constructed that incorporates prior factors, motion factors, cooperative observation factors, and LSTM prediction factors. The Levenberg–Marquardt algorithm is then used to solve the global optimization problem, producing the optimized state sequence for the slave AUV.

Algorithm 2: Post-Processing Cooperative Localization Algorithm Based on Factor Graph Optimization (UKF + LSTM + FG)

Input: Preliminary localization sequence of slave AUV, communication status sequence, trajectory of master AUV, LSTM prediction covariance
Output: Optimized state sequence of slave AUV $\{X_0^*, X_1^*, \cdots, X_k^*\}$

Initialization: Construct the variable node set $\chi = \{X_0, X_1, \cdots, X_k\}$
Add prior factor: $f_{prior}(X_0) \propto \exp(-\frac{1}{2} \parallel X_0 - \hat{X}_0 \parallel^2_{P_0})$
For $k = 0$ to $k = K - 1$ **do**
  Add motion factor: $f_{motion}(X_k, X_{k+1}) \propto \exp(-\frac{1}{2} \parallel e_k^{motion} \parallel^2_{Q_{motion}})$
For $k = 0$ to $k = K$ **do**
  If $c_k = 1$ (communication is normal) **then**
    Add cooperative observation factor: $f_{coop}(p_k) \propto \exp\left\{-\frac{1}{2} \parallel e_k^{coop} \parallel^2_{R_{coop}}\right\}$
  Else if $c_k = 0$ (communication is interrupted) **then**
    Add LSTM prediction factor: $f_{LSTM}(p_k) \propto \exp\left\{-\frac{1}{2} \parallel e_k^{lstm} \parallel^2_{R_{lstm}}\right\}$
$\chi^* = \underset{\chi}{\operatorname{argmin}}(\parallel X_0 - \hat{X}_0 \parallel^2_{P_0} + \sum_{k=0}^{T-2} \parallel e_k^{motion} \parallel^2_{Q_{motion}} + \sum_{k=0}^{T-1} \parallel e_k^{obs} \parallel^2_{R_{obs}(c_k)})$
Solve iteratively using Levenberg-Marquardt algorithm
End Return the optimized state sequence of slave AUV $\{X_0^*, X_1^*, \cdots, X_k^*\}$

Algorithms 1 and 2 together form a complete AUV swarm cooperative localization solution suitable for practical engineering requirements in underwater AUV swarm operations.

5. Simulation Experiments and Analysis

5.1. Experimental Setup

To verify the effectiveness of the AUV swarm cooperative localization method proposed in this paper, which combines LSTM-based prediction with factor graph optimization, a triangular 3D formation was simulated. This formation consisted of one master AUV and three slave AUVs. The starting coordinates are as follows: Master AUV: (0 m, 0 m, −30 m); Slave AUV-1: (−15 m, 26 m, −35 m); Slave AUV-2: (−15 m, −26 m, −35 m); Slave AUV-3: (30 m, 0 m, −35 m). The master AUV moves along a "lawnmower" scanning trajectory, covering a rectangular area measuring 500 m wide by 3000 m long. Its trajectory includes both constant-speed straight-line motion and turning and is represented by a black curve. The slave AUVs achieve coordinated swarm movement by maintaining their relative positions to the master AUV. Their trajectories are represented by green, pink, and blue lines, respectively. The movement trajectory and formation of the entire swarm are shown in Figure 7.

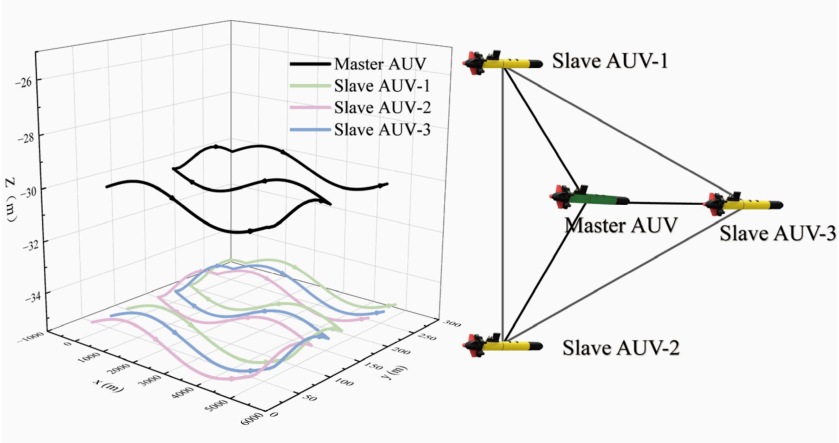


Figure 7. Movement Trajectories and Formation Configurations of the AUVs.

To address the problem of optimizing localization trajectories during communication interruptions in the AUV swarm, the simulation was run for 1500 s with a time step of 1 s. The initial states of each AUV were provided by GNSS or the mother ship. Between 900 and 1100 s, communication with the slave AUV was interrupted; during this period, the slave AUV could not receive any measurement data from the master AUV, and communication quality dropped to zero. The interruption interval was selected prior to a turn in the trajectory to verify the algorithm's robustness under nonstationary motion conditions. Upon completion of the simulation, localization data from the slave AUV obtained via real-time localization using the UKF + LSTM algorithm were used as the dataset for post-processing optimization experiments. Global optimization was performed using RTS smoothing and factor graph optimization, respectively.

To verify the effectiveness of the proposed cooperative localization algorithm under communication interruption conditions, the algorithm's performance is evaluated by comparing the AUV swarm's localization accuracy before and after optimization. Specifically, the Average Localization Error (ALE), Root Mean Square Error (RMSE) and Maximum

Error-to-Range Ratio (MER) during the communication interruption period are used as evaluation metrics to quantify improvements in localization accuracy.

$$RMSE = \sqrt{\frac{1}{T}\sum_{k=1}^{T}(LE_k)^2} \tag{35}$$

$$ALE = \frac{1}{T}\sum_{k=1}^{T} LE_k \tag{36}$$

$$LE_k = \sqrt{(x_k - x_{k|k})^2 + (y_k - y_{k|k})^2 + (z_k - z_{k|k})^2} \tag{37}$$

$$MER = \frac{\max\limits_{1\le k\le T} LE_k}{D_{path}} \times 100\% \tag{38}$$

In the equation, (x_k, y_k, z_k) represents the precise position of the AUV; $(x_{k|k}, y_{k|k}, z_{k|k})$ represents the estimated position at time k based on cooperative localization; LE_k represents the localization error at time k; T represents the length of the experimental data and D_{path} represents the actual distance traveled by the AUV during the communication interruption.

5.2. Experimental Analysis

Experiment 1: Comparative Experiment of Cooperative Localization Algorithms for AUV Swarm

To verify the effect of cooperative information fusion on localization accuracy during communication interruptions, this experiment compares four localization algorithms: UKF, UKF + LSTM, UKF + LSTM + RTS smoothing, and the UKF + LSTM + FG algorithm proposed in this paper. The initial localization state errors were set as follows: initial position error [1 m, 1 m, 1 m], initial velocity error [0.5 m/s, 0.5 m/s, 0.5 m/s], and initial acceleration error [0.1 m/s^2, 0.1 m/s^2, 0.1 m/s^2]. Process noise errors are set to [1 m, 0.5 m/s, 0.1 m/s^2], and measurement noise errors are set to [2 m, 0.5°, 0.3°]. The LSTM network architecture follows the design proposed in References [9,11], containing three layers with 32 hidden units per layer and a dropout rate of 0.2. The model takes range, azimuth, and elevation measurements of the past 15-time steps as inputs to predict the measurement at the next time step. MC Dropout is used to quantify model uncertainty, with 30 stochastic forward passes per inference.

Training samples are constructed online during localization. At each time step, consecutive 15-step subsequences are extracted from the measurement buffer and paired with the subsequent measurement as the learning target. Each input–target pair is independently Z-score normalized using the mean and standard deviation derived from its own 16-time-point window, enabling the network to learn relative temporal variations instead of absolute measurement magnitudes. All normalized pairs at each time step form a single batch for one gradient update using the Adam optimizer with a learning rate of 0.001 and mean squared error loss. The buffer stores 65 measurements, discarding the oldest value when full to maintain a fixed sliding window. The 50-step data margin beyond the 15-step input window ensures stable normalization statistics. Training initiates after 25 valid measurements have been accumulated and runs incrementally at each subsequent time step.

The experiment did not employ the traditional division of data into training, validation, and test sets. The localization data follow a strict chronological order; shuffling or fixed partitioning would disrupt the sequence dependencies for LSTM learning. Additionally, the task begins with no data, and the number of samples grows dynamically as the task progresses, making it impossible to use a fixed dataset partitioning scheme throughout the process. Therefore, all historical data was used for incremental online training. To evaluate

the model's generalization performance, this experiment conducted 100 independent Monte Carlo simulations. Each trial was initialized with different random seeds to independently generate process noise, measurement noise, and initial state errors. This yields unbiased statistics across runs while preventing training data leakage during evaluation.

A typical result from the 100 independent Monte Carlo simulations was selected for analysis. During the communication interruption period, a comparison of the slave AUV's localization trajectories under different algorithms with the true trajectory is shown in Figure 8. By comparing the degree of alignment between each algorithm's trajectory and the true trajectory, the effectiveness of the optimized algorithm is verified. Furthermore, the localization error sequences for each algorithm are illustrated in Figure 9, providing a comprehensive assessment.

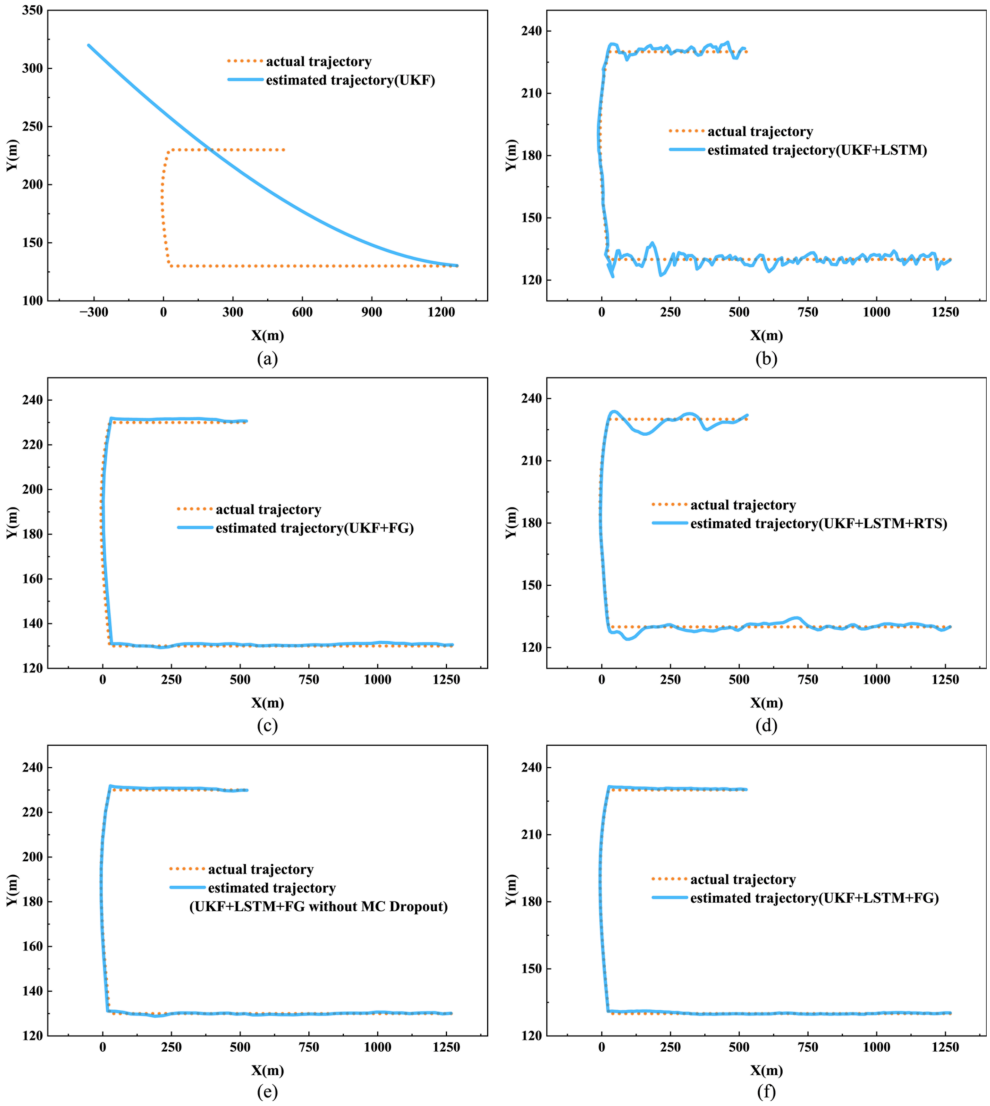


Figure 8. Comparison of the slave AUV's estimated trajectory and actual trajectory under different algorithms. (**a**) UKF algorithm; (**b**) UKF + LSTM algorithm; (**c**) UKF + FG algorithm; (**d**) UKF + LSTM + RTS algorithm; (**e**) UKF + LSTM + FG without MC Dropout algorithm; (**f**) UKF+LSTM+FG algorithm.

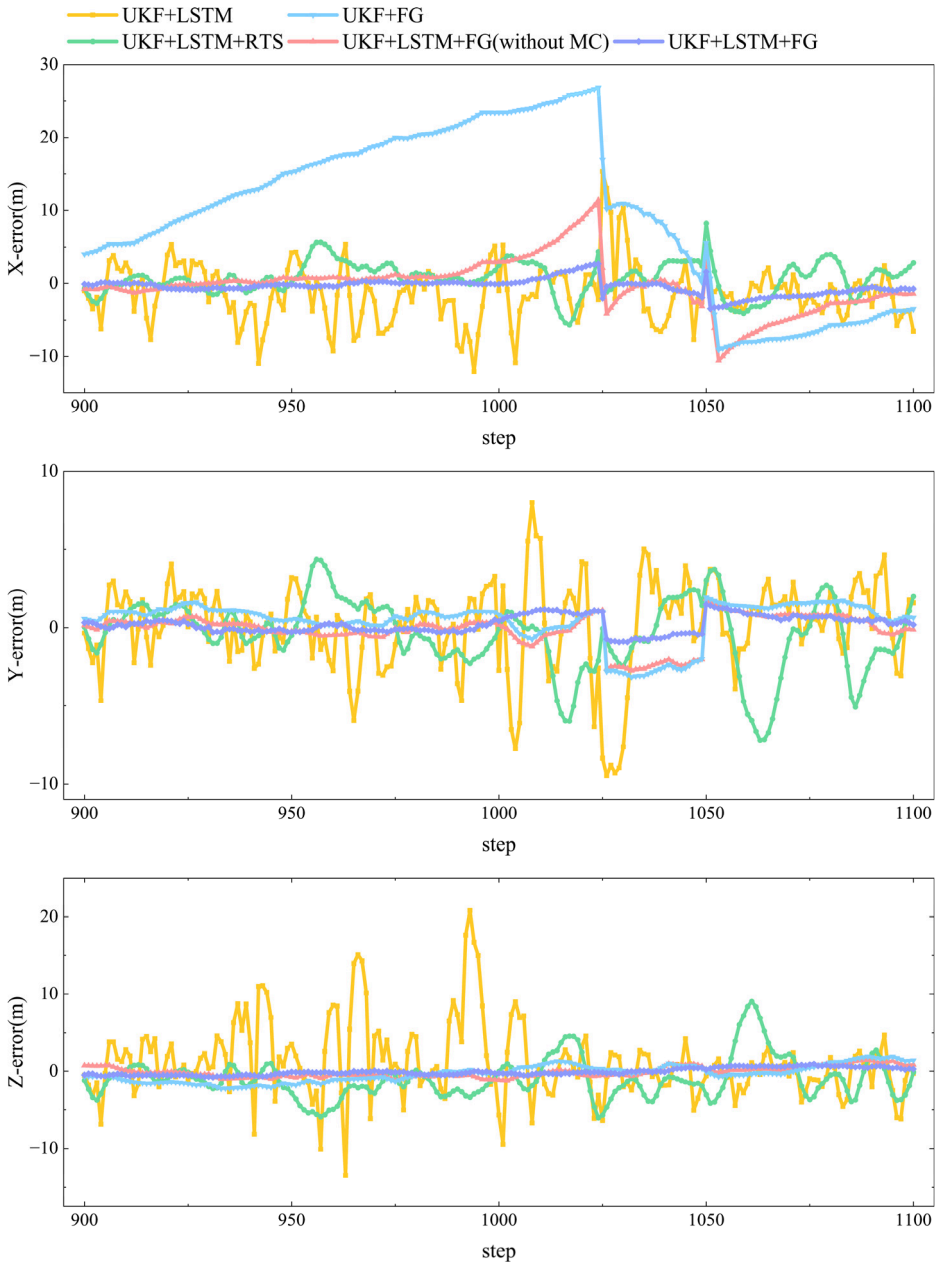


Figure 9. Sequence of localization errors for the slave AUV under different algorithms.

Figure 8a,b show that during communication interruptions, the trained LSTM model uses historical data to predict measurement information, effectively limiting the divergence of localization errors. This maintains continuity in the AUV swarm's cooperative localization system. Figures 8c and 9 show that when the UKF + FG algorithm lacks cooperative observations, it relies solely on motion-model constraints for post-processing the factor graph. The optimized trajectories deviate significantly. As shown in Figure 8c,d and Figure 9, both RTS smoothing and factor graph optimization use the UKF + LSTM estimation results as initial values during post-processing, thereby further improving localization accuracy through global optimization. Among these, the factor graph optimization algorithm achieves higher localization accuracy than RTS smoothing. This is because RTS smoothing performs backward recursion based on the UKF estimation results; essentially, it smooths the filtered trajectory, and its optimization is limited by accumulated errors from the forward filtering process. In contrast, factor graph optimization constructs a global factor graph to uniformly model motion constraints, actual cooperative observations

during normal communication, and LSTM-predicted observations during communication interruptions across the entire motion interval. By more fully utilizing available information to perform global optimization over the entire trajectory, it achieves superior localization accuracy.

Comparing Figure 8e,f shows that algorithms without uncertainty weighting treat all predicted observations equally. When prediction errors are significant at certain time points, this affects post-processing optimization of the localization trajectory, leading to increased localization errors. In contrast, the algorithm proposed in this paper improves the LSTM network using the MC Dropout method, which adaptively adjusts the confidence of LSTM prediction factors in the factor graph. This demonstrates that the uncertainty-weighted strategy fully mitigates the adverse effects of low-quality predictions on global optimization, thereby fully demonstrating its crucial role in enhancing fusion accuracy and algorithmic robustness. Statistical analysis was conducted based on 100 Monte Carlo simulations. A comparison of the localization accuracy metrics (ALE, RMSE, and their mean (Mean), standard deviation (Std), and 95% confidence interval (95%CI)) for each algorithm is shown in Table 1.

Table 1. Comparison of Localization Errors Among Different Cooperative Localization Methods During Communication Interruptions.

Methods	ALE/m	RMSE/m
	Mean ± Std [95% CI]	**Mean ± Std [95% CI]**
UKF	/	/
UKF + FG	12.12 ± 1.59 [11.79, 12.44]	13.38 ± 1.68 [13.05, 13.71]
UKF + LSTM	7.69 ± 6.28 [6.43, 8.90]	11.20 ± 10.60 [9.12, 13.27]
UKF + LSTM + RTS	5.42 ± 5.21 [4.38, 6.45]	7.98 ± 8.81 [6.25, 9.73]
UKF + LSTM (no MC) + FG	4.32 ± 1.44 [4.04, 4.60]	5.25 ± 1.35 [4.98, 5.51]
UKF + LSTM + FG	3.46 ± 1.25 [3.22, 3.71]	4.43 ± 1.23 [4.19, 4.67]

As shown in Table 1, the UKF algorithm displays error divergence during communication interruptions and is unable to provide effective localization results. The UKF + FG algorithm's ALE of 12.12 m and RMSE of 13.38 m indicate relatively high error levels. After introducing LSTM real-time prediction, the ALE of the UKF + LSTM algorithm decreased to 7.69 m, and the RMSE decreased to 11.20 m. Compared to the UKF + FG algorithm, the ALE and RMSE were reduced by 36% and 16%, respectively, demonstrating that LSTM prediction can suppress error divergence during communication interruptions. Compared to the cooperative localization results of the UKF + LSTM algorithm, the ALE was reduced by 29% and the RMSE by 28% after RTS smoothing. After factor graph optimization, the ALE was reduced by 55% and the RMSE by 60%. Experimental results show that after solving using the proposed UKF + LSTM + FG algorithm, the AUV's localization accuracy during communication interruption was significantly improved, verifying the effectiveness of factor graph optimization. Comparing the factor graph optimization algorithm with and without uncertainty weighting, after improving the LSTM network with MC Dropout, the algorithm's ALE and RMSE were reduced by 19% and 15%, respectively, and it exhibited a smaller standard deviation and narrower confidence intervals. This confirms that the uncertainty weighting strategy effectively suppresses the interference of low-quality predictions on global optimization, enhancing the algorithm's accuracy and robustness.

Experiment 2: Robustness Experiment of Cooperative Localization Algorithms Under Different Communication Interruption Durations

To further analyze the robustness of the factor graph optimization algorithm under different communication interruption durations, a comparative experiment was designed.

Communication interruption durations were set to 50 s, 100 s, 200 s, 300 s, and 400 s to analyze their impact on localization accuracy. To more clearly compare the cooperative localization algorithms, box plots were generated and the RMSE of localization error sequences was calculated for the three algorithms, UKF + LSTM, UKF + LSTM + RTS, and UKF + LSTM + FG, during underwater communication interruptions, as shown in Figure 10. Detailed statistical results are presented in Table 2.

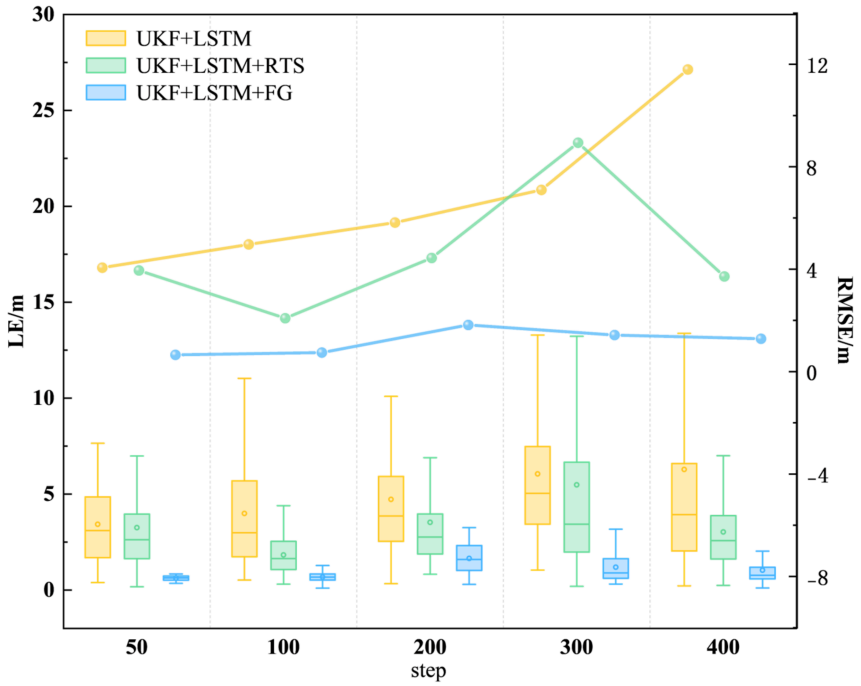


Figure 10. Box plots and RMSE of the localization error sequences for the cooperative localization algorithm.

Table 2. Statistical Results of Localization Errors for Different Cooperative Localization Methods During Communication Interruptions.

Interruption Time/s	UKF + LSTM		UKF + LSTM + RTS		UKF + LSTM + FG	
	RMSE/m	MER/%	RMSE/m	MER/%	RMSE/m	MER/%
50	4.04	1.97	3.94	1.92	0.63	0.17
100	4.92	1.77	2.07	0.44	0.72	0.13
200	5.81	1.13	4.42	0.73	1.80	0.17
300	7.08	0.90	8.93	1.74	1.41	0.13
400	11.79	2.16	3.70	0.40	1.26	0.09

Table 2 lists the localization results of the three algorithms for different interruption durations, including RMSE and MER. A comparative analysis shows that as communication interruption time increases, the RMSE of the UKF + LSTM algorithm rises from 4.04 m to 11.79 m. This is due to inherent uncertainty in the LSTM network during online training, causing localization errors to accumulate as travel distance increases. The localization accuracy of the RTS smoothing algorithm is generally better than that of the UKF + LSTM algorithm; however, it shows fluctuations as interruption duration increases. When the interruption duration is 300 s, the RMSE is 8.93 m; when it is 400 s, the RMSE is 3.70 m. This indicates that RTS can suppress forward filtering errors to some extent through reverse smoothing; however, its performance is influenced by error distribution, leading to instability. The factor graph optimization algorithm demonstrates the best and most stable localization accuracy across all interruption durations. Its RMSE values are

consistently lower than those of the other methods, indicating that it can effectively handle communication interruptions of varying durations and is highly robust. Its MER is better than 0.2% of the range.

6. Conclusions

This paper addresses cumulative localization errors in AUV swarms caused by interruptions in underwater acoustic communication by proposing a cooperative localization method based on LSTM prediction and factor graph optimization. By integrating the LSTM prediction network with the factor graph optimization framework, this method corrects AUV trajectories during communication interruptions. On the AUV swarm leader node, a joint factor graph comprising motion model factors, cooperative ranging factors, and LSTM prediction factors is constructed by adaptively switching factor types based on communication status. This approach fully utilizes available historical observations and predictive information to obtain optimal state estimates for AUVs. Simulation results show that the proposed method adopts a two-stage processing strategy combining online filtering with offline optimization, and can solve the cooperative localization problem of AUV swarms with high accuracy and robustness under communication interruptions. Future work will focus on extending the algorithm to full-state-space modeling and validating it with actual test data, further exploring mechanisms for robust cooperative localization enhancement and scenario-adaptive optimization tailored to complex missions, to continuously improve the method's adaptability and engineering applicability in real marine environments.

Author Contributions: Conceptualization, W.X.; Methodology, T.S.; Formal analysis, T.S. and Y.D.; Software, T.S. and J.L.; Writing—original draft preparation, T.S.; Writing—review and editing, T.S. and W.X. All authors have read and agreed to the published version of the manuscript.

Funding: This work was supported by the National Natural Science Foundation of China (61071006).

Data Availability Statement: The original contributions presented in this study are included in the article. Further inquiries can be directed to the corresponding author.

Conflicts of Interest: The authors declare no conflicts of interest.

References

1. Zhou, J.; Si, Y.; Chen, Y. A review of subsea AUV technology. *J. Mar. Sci. Eng.* **2023**, *11*, 1119. [CrossRef]
2. Du, Z.; Chai, H.; Xiang, M.; Zhang, F.; Wang, Z. Resilient model of multi-UUVs cooperative localization for detection of sensor fault and outliers. *Ocean Eng.* **2022**, *266*, 113216. [CrossRef]
3. Chen, T.; Zhang, Z.; Fang, Z.; Jiang, D.; Li, G. Imitation learning from imperfect demonstrations for AUV path tracking and obstacle avoidance. *Ocean Eng.* **2024**, *298*, 117287. [CrossRef]
4. Song, B.W.; Pan, G.; Zhang, L.C.; Huang, Q.G.; Yu, Y.; Tian, W.L.; Dong, H.C.; Zhang, X.H. Development trend and key technologies of autonomous underwater vehicles. *Chin. J. Ship Res.* **2022**, *17*, 27–44. [CrossRef]
5. Ma, X.; Li, C. Research on AUVs parallel cooperative navigation and localization technology based on factor graph. In *2024 18th International Conference on Ubiquitous Information Management and Communication (IMCOM)*; IEEE: Piscataway, NJ, USA, 2024; pp. 1–7. [CrossRef]
6. Yan, H.; Liu, S.; Pan, C.; Kuang, B.; Wang, S.; Qiao, G. Simulation of non-stationary mobile underwater acoustic communication channels based on a multi-scale time-varying multipath model. *J. Mar. Sci. Eng.* **2025**, *13*, 1765. [CrossRef]
7. Xu, B.; Li, S.X.; Wang, L.Z.; Duan, T.H.; Yao, H. A multi-AUV cooperative localization method based on adaptive neuro-fuzzy inference system. *J. Chin. Inert. Technol.* **2019**, *27*, 440–447. [CrossRef]
8. Xu, B.; Li, S.X.; Razzaqi, A.A.; Wang, L.Z.; Jiao, M.Y. A novel ANFIS-AQPSO-GA-based online correction measurement method for cooperative localization. *IEEE Trans. Instrum. Meas.* **2022**, *71*, 1–17. [CrossRef]
9. Li, J.; Tian, Z.; Zhang, G.; Li, W. Multi-AUV formation predictive control based on CNN-LSTM under communication constraints. *J. Mar. Sci. Eng.* **2023**, *11*, 873. [CrossRef]
10. Xu, B.; Wang, X.; Zhang, J.; Guo, Y.; Razzaqi, A.A. A novel adaptive filtering for cooperative localization under compass failure and non-Gaussian noise. *IEEE Trans. Veh. Technol.* **2022**, *71*, 3737–3749. [CrossRef]

11. Sun, T.; Xu, W.M.; Yan, Q. An LSTM-based cooperative localization algorithm for AUV swarms. *Hydrogr. Surv. Chart.* **2025**, *45*, 63–67. [CrossRef]
12. Zhang, L.; Wu, W.Q.; Wang, M.S. Application of state transformation extended Kalman smoothing in AUV underwater track correction. *J. Chin. Inert. Technol.* **2020**, *28*, 206–212. [CrossRef]
13. Luo, Y.R.; Guo, W.F.; Qi, S.F.; Guo, C. Invariant RTS smoother and its application in 5G/SINS integrated navigation system. *Geomat. Inf. Sci. Wuhan Univ.* **2022**, *49*, 747–755. [CrossRef]
14. Dong, Q.W.; Yue, C.Q.; Wang, A.B.; Wang, T.T. A post-processing method of navigation data for leader AUV based on backward calculating. *J. Unmanned Undersea Syst.* **2020**, *28*, 420–427. [CrossRef]
15. Wu, Q.; Chai, H.Z.; Bai, S.Y.; Xiang, M.Z.; Ma, H.L.; Zhang, F. Application of a hybrid RTS and FBC post-processing smoothing algorithm in AUV underwater positioning. *J. Beijing Univ. Aeronaut. Astronaut.* **2025**, *51*, 1–17. [CrossRef]
16. Ma, X.; Liu, X.; Li, C.; Sheng, G. A post-processing algorithm based on factor graph optimization for autonomous underwater vehicle integrated navigation. *Trans. Inst. Meas. Control* **2022**, *45*, 595–607. [CrossRef]
17. Wang, D.; Lian, B.; Liu, Y.; Gao, B.; Zhang, S. Resilient cooperative localization based on factor graphs for multirobot systems. *Remote Sens.* **2024**, *16*, 832. [CrossRef]
18. Wang, M.; Li, L.; Liu, J.; Chen, R. Neural network aided factor graph optimization for collaborative pedestrian navigation. *IEEE Trans. Intell. Transp. Syst.* **2023**, *25*, 303–314. [CrossRef]
19. Zhang, L.C.; Qu, J.Q.; Pan, G.; Wang, Y.Z. Analyzing of cooperative locating error and formation configuration of AUV based on geometric interpretation. *J. Northwest. Polytech. Univ.* **2020**, *38*, 755–765. [CrossRef]
20. Sun, D.J.; Zhang, Y.N.; Han, Y.F.; Zhang, J.C. Preliminary study on cooperative localization for AUVs. In *2017 IEEE International Conference on Signal Processing, Communications and Computing (ICSPCC)*; IEEE: Piscataway, NJ, USA, 2017; pp. 1–4. [CrossRef]
21. Allotta, B.; Chisci, L.; Costanzi, R.; Fanelli, F.; Fantacci, C.; Meli, E.; Ridolfi, A.; Caiti, A.; Di Corato, F.; Fenucci, D. A comparison between EKF-based and UKF-based navigation algorithms for AUVs localization. In *OCEANS 2015—Genova*; IEEE: Piscataway, NJ, USA, 2015; pp. 1–5. [CrossRef]
22. Tian, K.; Radovnikovich, M.; Cheok, K. Comparing EKF, UKF, and PF performance for autonomous vehicle multi-sensor fusion and tracking in highway scenario. In *2022 IEEE International Systems Conference (SysCon)*; IEEE: Piscataway, NJ, USA, 2022; pp. 1–6. [CrossRef]
23. Amin Maleki Sadr, M.; Zhu, Y.; Hu, P. An anomaly detection method for satellites using Monte Carlo dropout. *IEEE Trans. Aerosp. Electron. Syst.* **2023**, *59*, 2044–2052. [CrossRef]
24. Zhu, J.; Li, A.; Qin, F.; Chang, L.; Qian, L. A hybrid method for dealing with DVL faults of SINS/DVL integrated navigation system. *IEEE Sens. J.* **2022**, *22*, 15844–15854. [CrossRef]
25. Bucci, A.; Franchi, M.; Ridolfi, A.; Secciani, N.; Allotta, B. Evaluation of UKF-based fusion strategies for autonomous underwater vehicles multisensor navigation. *IEEE J. Ocean. Eng.* **2023**, *48*, 1–26. [CrossRef]
26. Fernandes, M.; Sahoo, S.R.; Kothari, M. Cooperative localization for autonomous underwater vehicles—A comprehensive review. *arXiv* **2023**, arXiv:2307.06189. [CrossRef]
27. Li, S.; López-Benítez, M.; Lim, E.G.; Ma, F.; Cao, M.; Yu, L.; Qin, X. Enabling cooperative autonomy in UUV clusters: A survey of robust state estimation and information fusion techniques. *Drones* **2025**, *9*, 752. [CrossRef]
28. Fischer, A.; Izmailov, A.F.; Solodov, M.V. The Levenberg–Marquardt method: An overview of modern convergence theories and more. *Comput. Optim. Appl.* **2024**, *89*, 33–67. [CrossRef]

Disclaimer/Publisher's Note: The statements, opinions and data contained in all publications are solely those of the individual author(s) and contributor(s) and not of MDPI and/or the editor(s). MDPI and/or the editor(s) disclaim responsibility for any injury to people or property resulting from any ideas, methods, instructions or products referred to in the content.